

CHAPTER 98

ROCK SLOPES UNDER IRREGULAR WAVE ATTACK

Nobuhisa Kobayashi¹, Andojo Wurjanto², and Daniel T. Cox³

ABSTRACT

The numerical model that was shown to be in fair agreement with six test runs of available data on the stability of rock units under irregular wave attack is used to examine the critical incident wave profile associated with the minimum rock stability for each run. The minimum rock stability computed for the runs with dominant plunging waves on gentler slopes is caused by the large wave with the maximum crest elevation during its uprush on the slope. The minimum rock stability computed for the runs with dominant surging waves on steeper slopes is caused by the downrushing water with high velocities resulted from a large zero-upcrossing wave with a high crest followed by a deep trough. In addition, a simplified model is proposed to predict the eroded area due to the movement and dislodgement of rock units using the probability of armor movement computed by the numerical model. This model is shown to be in qualitative agreement with the empirical formula of Van der Meer (1988).

INTRODUCTION

Kobayashi and Wurjanto (1989a) synthesized their numerical models and presented a computer program called IBREAK, which may be used for the design of rough or smooth impermeable coastal structures of arbitrary geometry against normally incident waves. Kobayashi and Wurjanto (1989c) showed that IBREAK could be calibrated and applied to predict the hydrodynamic forces and sliding motion of dolos units at the Crescent City breakwater. Kobayashi, Cox and Wurjanto (1990) conducted irregular wave tests and showed that IBREAK could be extended to predict irregular wave reflection and runup on a 1:3 rough impermeable slope. On the other hand, Kobayashi and Wurjanto (1989b, 1990) extended IBREAK to predict the flow and armor response on a rough permeable slope as well as the flow in a thin permeable underlayer. Kobayashi, Wurjanto and Cox (1990) applied the extended numerical model and showed that the computed critical stability number for initiation of rock movement under the computed irregular wave motion was in good agreement with the stability number corresponding to the start of damage measured by Van der Meer (1988).

¹Assoc. Prof., Center for Applied Coastal Research, Dept. of Civil Engrg., Univ. of Delaware, Newark, DE 19716

²Graduate Student, Dept. of Civil Engrg., Univ. of Delaware, Newark, DE 19716

³Graduate Student, Dept. of Civil Engrg., Kyoto Univ., Kyoto 606, Japan

In this paper, the temporal and spatial variations of the stability of rock units computed by Kobayashi, Wurjanto and Cox (1990) are analyzed in detail to examine what wave conditions may cause the minimum stability of rock units. Gunbak and Bruun (1979) described the various sequences of waves which may cause severe conditions on a breakwater. Their descriptions were qualitative since it is very difficult to measure the flow and armor response simultaneously.

COMPARISON BETWEEN MEASURED AND COMPUTED STABILITY NUMBERS

In the following, the comparison made by Kobayashi, Wurjanto and Cox (1990) is summarized. They expressed the hydraulic stability condition against sliding or rolling of an armor unit on a rough permeable slope in the form

$$N_s = H'(s - 1)^{-1}(\rho s/W')^{1/3} \leq N_R(t, x) \quad (1)$$

where N_s = stability number; H' = incident wave height used for the normalization of dimensional variables indicated by the prime; s = specific density of the armor unit; ρ = fluid density; W' = median mass of the armor units; and N_R = armor stability function. The dimensionless function N_R varies with the normalized time, $t = t'/T'$, and the normalized horizontal distance from the toe of the slope, $x = x'/[T'(gH')^{1/2}]$, where T' = incident wave period used for the normalization; and g = gravitational acceleration. The expression of N_R as a function of the normalized fluid velocity and acceleration was given in the paper of Kobayashi and Wurjanto (1990) where the input parameters for the computation of the armor stability were specified.

Computation was made for six test runs selected from the test results with the dimensionless damage level, $S=2$, and the number of incident waves, $N = 1000$, listed in Appendix II of the thesis of Van der Meer (1988). These runs corresponded to the start of damage. The incident irregular waves for the six runs were generated using the Pierson-Moskowitz spectrum. The significant wave height, H'_s , and the average period of the zero upcrossings, T'_m , of the incident wave train were used by Van der Meer to characterize the incident irregular waves. As a result, use was made of $H' = H'_s$ and $T' = T'_m$ for the normalization of the dimensional variables. The normalized incident wave train, $\eta_i(t) = \eta'_i/H'$, at the toe of the $1 : \cot \theta'$ slope required as input to the numerical model was generated numerically for the specified spectral density with assumed random phases. Since different sets of the random phases yield different temporal variations of $\eta_i(t)$, the incident irregular wave train specified for each run was not the same as that generated in a wave flume by Van der Meer (1988). In order to reduce the computation time, the duration of the computation was limited to $0 \leq t \leq 256$, corresponding to $N = 256$ instead of $N = 1000$.

Table 1 lists the values of $\cot \theta'$, $H' = H'_s$, $T' = T'_m$, $\xi = T' \tan \theta' / (2\pi H' / g)^{1/2}$ and N_s for each of the six test runs, where ξ = surf similarity parameter based on H'_s and T'_m . The six runs with $\xi = 1.72 - 6.88$ were selected to represent dominant breaker types of plunging, collapsing and surging waves on uniform slopes. Runs R2a and R2b corresponded to run R2 and were based on the same spectral density with given values of H'_s and T'_m . The time series $\eta_i(t)$ for runs R2a and R2b were generated numerically using different sets of the random phases.

Table 1 also lists the computed value of the critical stability number N_{sc} for each run. The value of N_{sc} for each run was taken as the minimum value

Table 1: Six Test Runs Compared with Numerical Model

Run No.	$\cot \theta'$	H' (cm)	T' (sec)	ξ	Measured N_s	Computed N_{sc}
R1	6	10.09	2.63	1.72	1.72	1.56
R2a	6	7.75	3.15	2.36	1.32	1.75
R2b	6	7.75	3.15	2.36	1.32	1.63
R3	4	8.16	3.22	3.52	1.39	1.15
R4	3	8.92	3.13	4.37	1.52	1.36
R5	2	7.98	2.69	5.95	1.36	1.01
R6	2	7.98	3.11	6.88	1.36	1.47

of $N_R(t, x)$ for the ranges of $x \geq 0$ and $8 \leq t \leq 256$ where the normalized horizontal coordinate x was taken to be positive landward with $x = 0$ at the toe of the slope and the duration $0 \leq t < 8$ was excluded to account for the initial transient waves in the computation starting from the initial conditions of no wave action in the region $x \geq 0$ at $t = 0$. The computed critical stability number N_{sc} and the measured stability number N_s are in fair agreement as shown in Table 1 where the values of N_{sc}/N_s are in the range 0.74-1.33. The small difference between the computed values of N_{sc} for runs R2a and R2b indicates the variability caused by the random phases, although a much larger number of simulated runs are required to perform a statistical analysis of the variability. The comparison between N_s and N_{sc} shown in Table 1 is not really rigorous because of the inherent differences between these stability numbers as discussed by Kobayashi, Wurjanto and Cox (1990).

WAVE CONDITIONS FOR CRITICAL ARMOR STABILITY

The wave conditions corresponding to the computed minimum stability of rock units for each run are examined in this paper to identify the wave conditions which are critical to the stability of rock units. In the following, runs R1 and R4 may be regarded as representative runs for dominant plunging and surging waves, respectively, whereas run R3 happens to include an exceptionally large wave.

The free surface displacement above the still water level (SWL) and the depth-averaged horizontal fluid velocity are normalized as $\eta = \eta'/H'$ and $u = u'/(gH')^{1/2}$, respectively, where u is taken to be positive landward. Fig. 1 shows the computed variations of η , u and N_R with respect to x at the time, $t = t_{sc}$, when the minimum value of N_R in the range $x \geq 0$ corresponds to the critical stability number N_{sc} . The values of t_{sc} for runs R1, R3 and R4 are 164.75, 156.38 and 161.55, respectively. The shaded area shown in the figure for η corresponds to the permeable underlayer for each test where the numerical model is presently limited to the case of a thin permeable underlayer (Kobayashi and Wurjanto, 1990). Fig. 1 also shows the computed variation of the local stability number N_{sx} with respect to x where N_{sx} was defined as the minimum value of $N_R(t, x)$ at the specified location during $8 \leq t \leq 256$. The minimum value of N_{sx} with respect to x equals the critical stability number N_{sc} .

The critical stability number for run R1 with $\xi = 1.72$ occurs slightly behind the steep front of the uprushing water with large upslope velocities and accel-

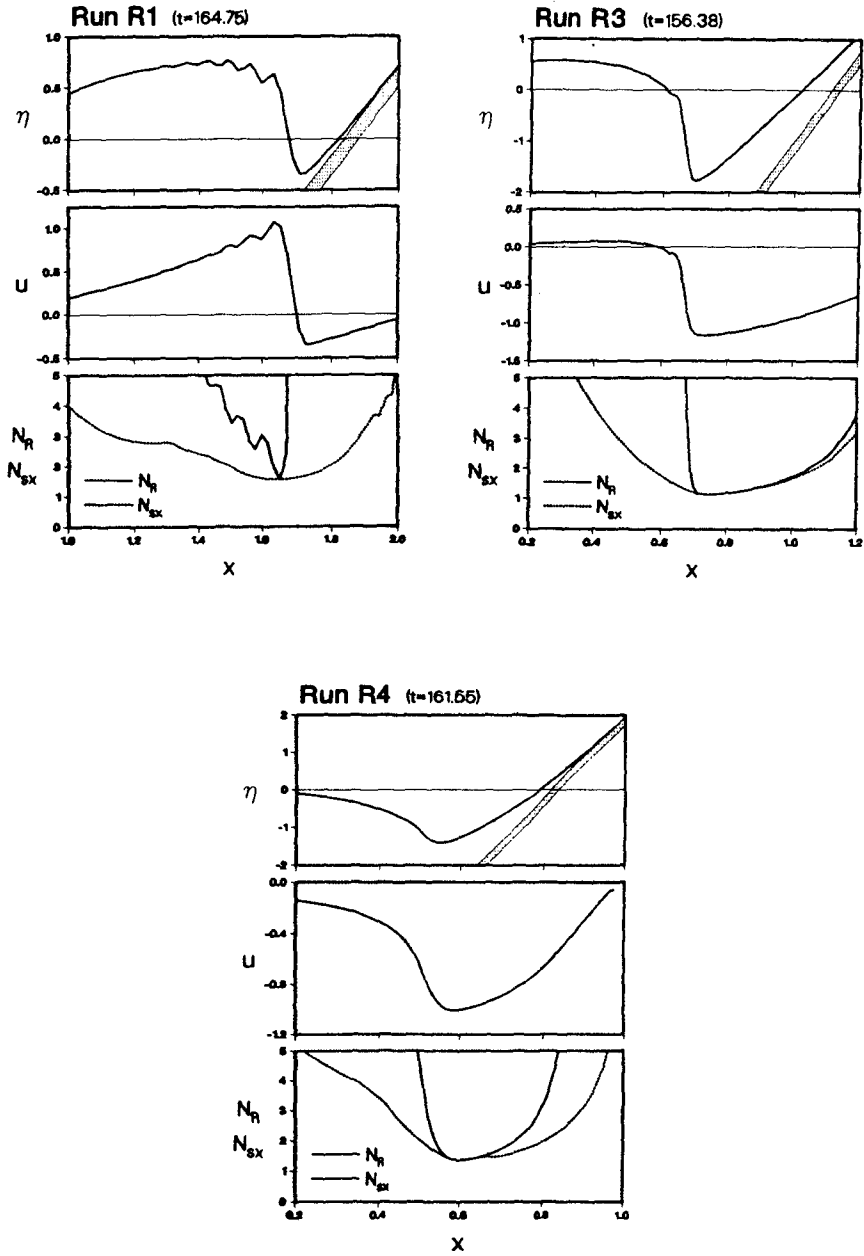


Figure 1: Variations of η , u and N_R with Respect to x at Time of Minimum Stability for Runs 1, 3 and 4

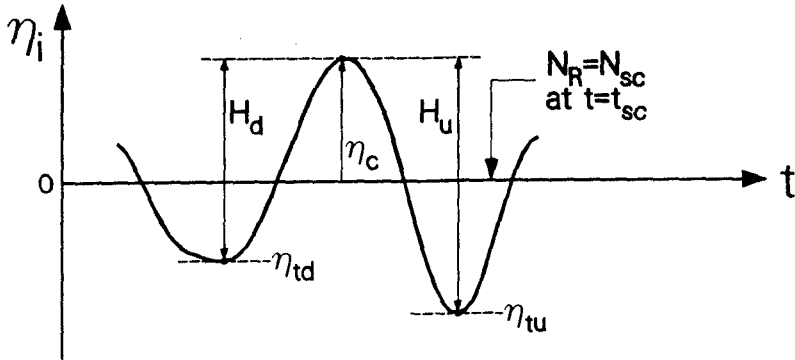


Figure 2: Definition Sketch for Critical Incident Wave Profile

erations. The local stability number in the range $1.5 \leq x \leq 1.9$ is computed to occur when this steep front moves upslope. On the other hand, the critical stability number for run R4 with $\xi = 4.37$ is caused by the downrushing water with large downslope velocities. For the exceptional case of run R3, the downrushing water flows extremely deep below SWL and encounters the uprushing water. The corresponding incident wave profile for run R3 will be shown to exhibit a very high crest followed by a very deep trough. This is one of the dangerous wave conditions identified by Gunbak and Bruun (1979).

The incident wave profile associated with the critical stability number N_{sc} for each run is examined to identify the incident wave profiles which may cause the critical uprushing or downrushing flow on uniform slopes. Fig. 2 shows the incident wave profile $\eta_i(t)$ at the toe of the slope normalized by the zero-upcrossing significant wave height H'_s slightly before the time $t = t_{sc}$ when $N_R(t, x) = N_{sc}$ at the certain location on the slope. The crest elevation η_c above SWL associated with the critical incident wave profile is obtained. The trough elevations η_{td} and η_{tu} adjacent to the crest elevation η_c are then found using the zero-downcrossing and zero-upcrossing methods, respectively. The corresponding wave heights H_d and H_u are given by $H_d = (\eta_c - \eta_{td})$ and $H_u = (\eta_c - \eta_{tu})$.

The values of η_c , η_{td} and η_{tu} for each run are listed in Table 2. These values are compared with the maximum crest elevation η_{cm} and the minimum trough elevation η_{tm} for $\eta_i(t)$ during $0 \leq t \leq 256$. Table 2 shows that $\eta_c = \eta_{cm}$ for runs R1, R2a, R2b and R3 while $\eta_{tu} = \eta_{tm}$ for runs R3 and R4. For runs R5 and R6, η_c is somewhat smaller than η_{cm} and η_{tu} is somewhat larger than η_{tm} .

Table 3 lists the values of H_d , T_d , H_u and T_u for each run where T_d and T_u are the zero-downcrossing and zero-upcrossing periods, respectively, of the individual wave whose crest elevation is η_c . The wave periods are normalized by the average zero-upcrossing period T'_m . Table 3 also lists the ranks of H_d and H_u among the 256 zero-downcrossing and zero-upcrossing individual wave heights, respectively, which are ranked in the descending order. Table 3 suggests that the critical incident wave profile is more related to the zero-upcrossing wave than the zero-downcrossing wave for runs R4, R5 and R6. The zero-upcrossing wave with $\eta_c = 1.052$, $\eta_{tu} = -1.126$ and $H_u = 2.178$ for run R3 appears to be exceptional, although the computed critical stability number N_{sc} for run R3 listed in Table 1 is not exceptionally small.

Table 2: Crest and Trough Elevations of Critical Wave Profile

Run	Crest		Trough		
No.	η_c	η_{cm}	η_{td}	η_{tu}	η_{tm}
R1	0.905	0.905	-0.527	-0.669	-0.934
R2a	0.822	0.822	-0.602	-0.459	-0.833
R2b	0.969	0.969	-0.877	-0.648	-0.933
R3	1.052	1.052	-0.673	-1.126	-1.126
R4	0.605	0.873	-0.034	-0.783	-0.783
R5	0.720	0.787	-0.550	-0.686	-0.793
R6	0.772	0.940	-0.447	-0.712	-0.974

Table 3: Wave Heights and Periods of Critical Wave Profile

Run No.	Zero-Downcrossing			Zero-Upcrossing		
	H_d	Rank	T_d	H_u	Rank	T_u
R1	1.433	4	1.263	1.575	1	1.256
R2a	1.424	3	1.195	1.280	7	1.518
R2b	1.846	1	1.189	1.617	3	1.116
R3	1.726	2	1.134	2.178	1	1.014
R4	0.639	118	0.649	1.388	5	1.213
R5	1.270	5	0.951	1.407	2	0.904
R6	1.219	17	1.066	1.484	4	1.235

Figs. 3-5 show the temporal variations of $\eta_i(t)$ and $Z_r(t)$ in the vicinity of $t = t_{sc}$ for runs R1, R3 and R4, respectively, where $Z_r = Z'_r/H'$ is the normalized waterline elevation on the slope above SWL corresponding to the instantaneous water depth $\delta'_r = 1$ cm (Kobayashi et al. 1990). Figs. 3-5 also show the zero-upcrossing and zero-downcrossing wave height distributions of the specified incident wave train $\eta_i(t)$ for each run as compared with the Rayleigh distribution given by $P = \exp[-2(H_p/H_s)^2]$ where P is the exceedance probability associated with the normalized wave height H_p and H_s is the normalized significant wave height.

The value of P for give H_p is estimated by $P = n/(N_o + 1)$ where $n =$ rank of H_p and $N_o =$ number of individual waves, which is 256 for these runs. Since the zero-upcrossing significant wave height H'_s is used for the normalization, $H_s = 1$ for the zero-upcrossing wave height distribution. The values of H_s for the zero-downcrossing wave height distribution are found to be essentially unity for all runs. Figs. 3-5 also point out the exceedance probability P for H_u and H_d for each of the three runs to indicate the values of H_u and H_d as compared with the rest of the individual wave heights.

Figs. 3-5 together with Figs. 1-2 and Tables 1-3 elucidate the critical wave conditions corresponding to the minimum stability of rock units for each run. For run R1 with $\cot \theta' = 6$ and $\xi = 1.72$, the critical stability number occurs at the time t_{sc} when the large wave with the maximum crest elevation $\eta_c = \eta_{cm}$ uprushes on the slope and encounters the trough of the waterline oscillation on the slope as shown in Fig. 3. The computed results for runs R2a and R2b with

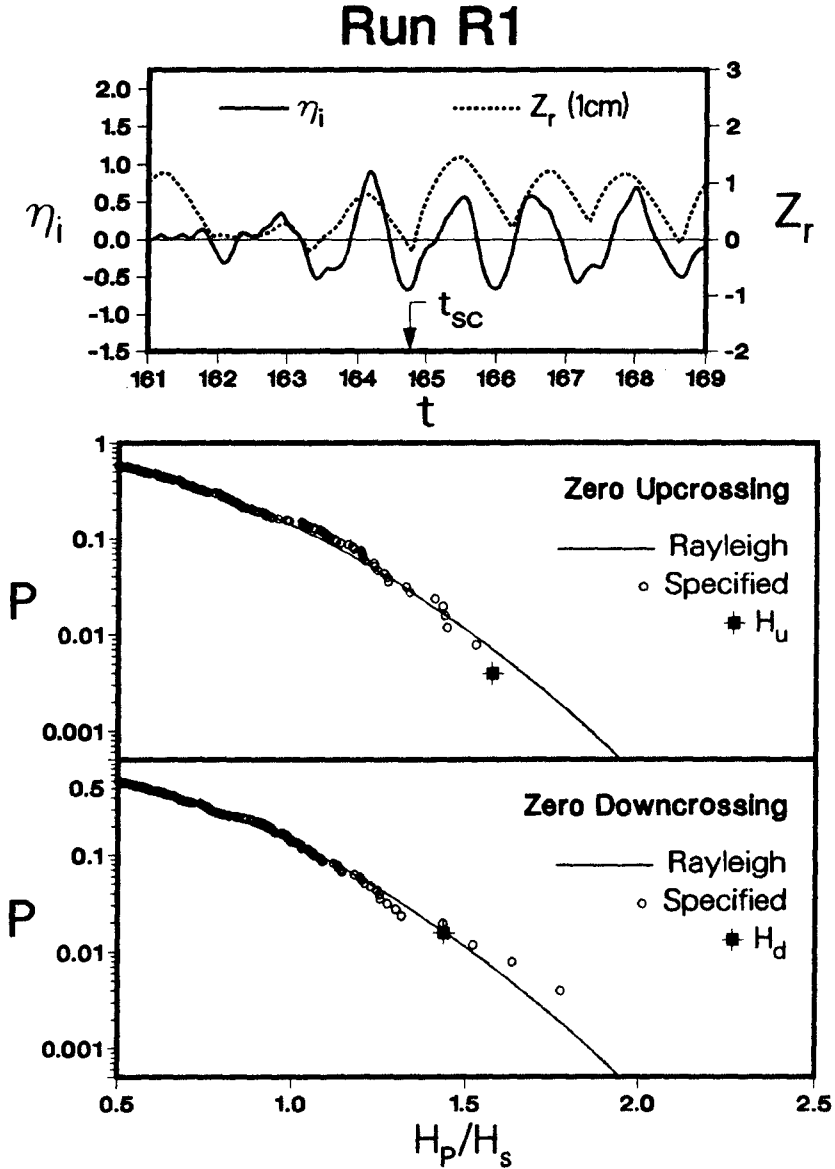


Figure 3: Analysis of Critical Wave Profile for Run R1

Run R3

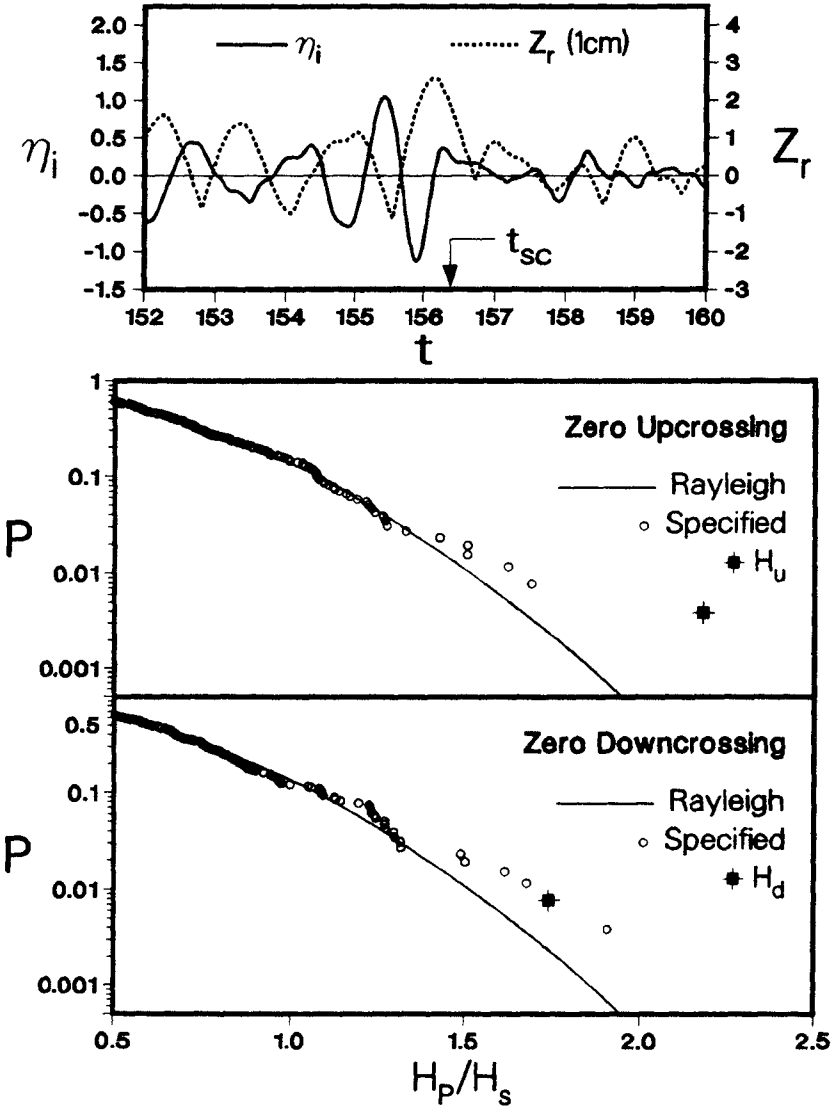


Figure 4: Analysis of Critical Wave Profile for Run R3

Run R4

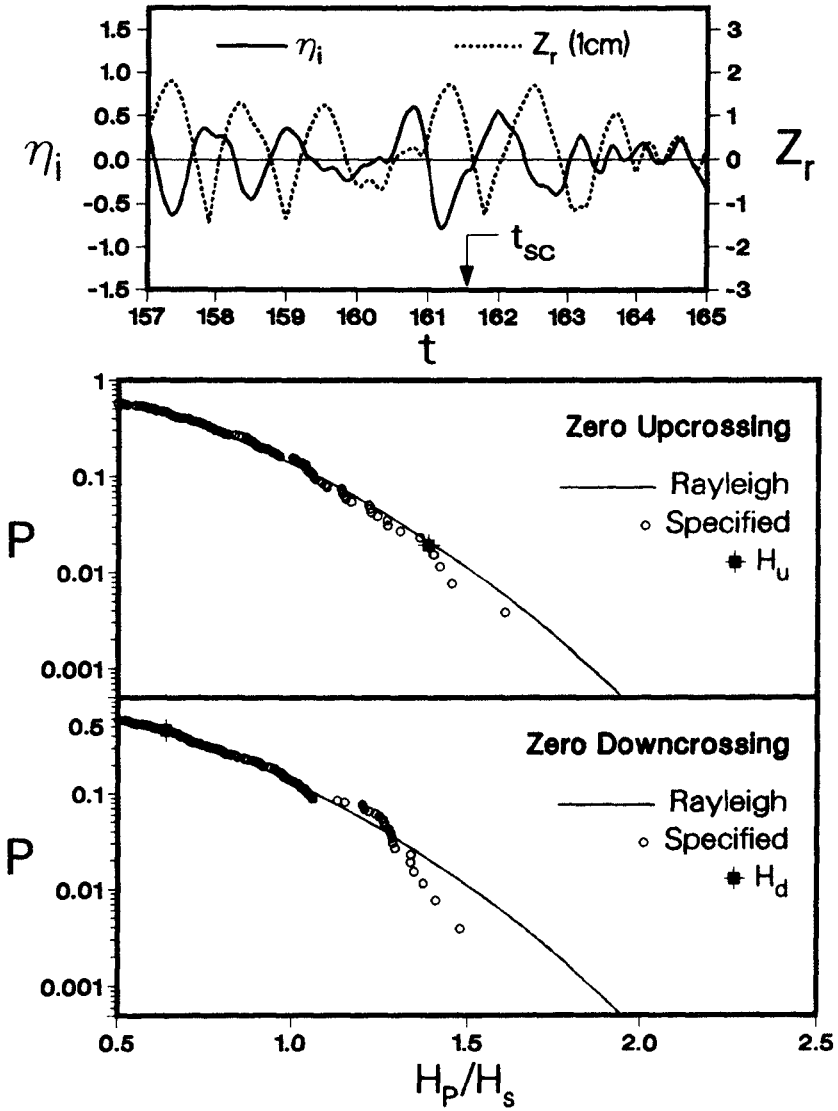


Figure 5: Analysis of Critical Wave Profile for Run R4

$\cot \theta' = 6$ and $\xi = 2.36$ are very similar to those for run R1. Additional runs are required to determine whether these critical wave conditions are limited to relatively gentle slopes such as $\cot \theta' = 6$ or can occur for steeper slopes as long as the surf similarity parameter is roughly two. For run R3 with $\cot \theta' = 4$ and $\xi = 3.52$, the critical stability number occurs at the time t_{sc} when the extremely large wave with the maximum crest elevation $\eta_c = \eta_{cm}$ and the minimum trough elevation $\eta_{tu} = \eta_{tm}$ causes the downrushing water with large velocities following large runup as shown in Fig. 4. For run R4 with $\cot \theta' = 3$ and $\xi = 4.37$, the critical stability number occurs at the time t_{sc} when the relatively large zero-upcrossing wave with the high crest followed by the deep trough causes the downrushing water with large velocities with the waterline on the slope being near SWL as shown in Fig. 5. The computed results for run R5 with $\cot \theta' = 2$ and $\xi = 5.95$ and run R6 with $\cot \theta' = 2$ and $\xi = 6.88$ are similar to those for run R4.

PROBABILITY OF ARMOR MOVEMENT AND DAMAGE LEVEL

The critical incident wave profile and resulting critical stability number N_{sc} is useful for the design of armor units in which $N_s < N_{sc}$ so that armor units will not move under the action of design waves. If the mass of armor units is reduced such that $N_s > N_{sc}$, the degree of armor movement and resulting profile change will need to be predicted.

The computed armor stability function $N_R(t, x)$ depends on the normalized incident wave train $\eta_i(t)$ and the slope and armor characteristics specified as input to the numerical model. In the numerical model, the constant friction factor f' is used to account for the roughness effects of the primary cover layer on the flow over the rough permeable slope, while the effects of the permeable underlayer are taken into account by the volume and momentum fluxes into or out of the permeable underlayer. Since the computed flow field is not very sensitive to the assumed value of f' , the computed temporal and spatial variations of $N_R(t, x)$ for each run in Table 1 may be assumed to remain essentially the same even if the stability number N_s defined in Eq. 1 is increased somewhat by decreasing only the median mass W' of the armor units.

In the following, the probability of armor movement based on the movement duration, P_t , and the probability of armor movement per unit normalized time, P_m , are predicted as a function of the stability number $N_s > N_{sc}$ and the location x of the armor unit along the uniform slope. For given N_s and x , armor movement will occur during the time when $N_s > N_R$. The duration of each event of armor movement is denoted by t_j with $j = 1, 2, \dots, J$ where $J =$ number of armor movement events during the specified duration $t_{min} \leq t \leq t_{max}$. In this paper $t_{min} = 8$ and $t_{max} = 256$. From the computed armor movement statistics, the probabilities P_t and P_m may be defined as

$$P_t = (t_{max} - t_{min})^{-1} \sum_{j=1}^J t_j ; P_m = \frac{J}{(t_{max} - t_{min})} \tag{2}$$

For example, Fig. 6 shows the computed probabilities P_t and P_m for $N_s/N_{sc} = 1.1, 1.3$ and 1.5 for run R1 where the normalized elevation, $z = z'/H'$, of the armor unit on the slope relative to SWL located at $z = 0$ is used instead of x . The computed probabilities of the armor movement occurring mostly below SWL increase with the increase of N_s . For run R1, the computed value of N_{sc} is 1.56 and the measured value of N_s corresponding to the start of the damage was 1.72 as listed in Table 1. This implies that the numerical model predicts the

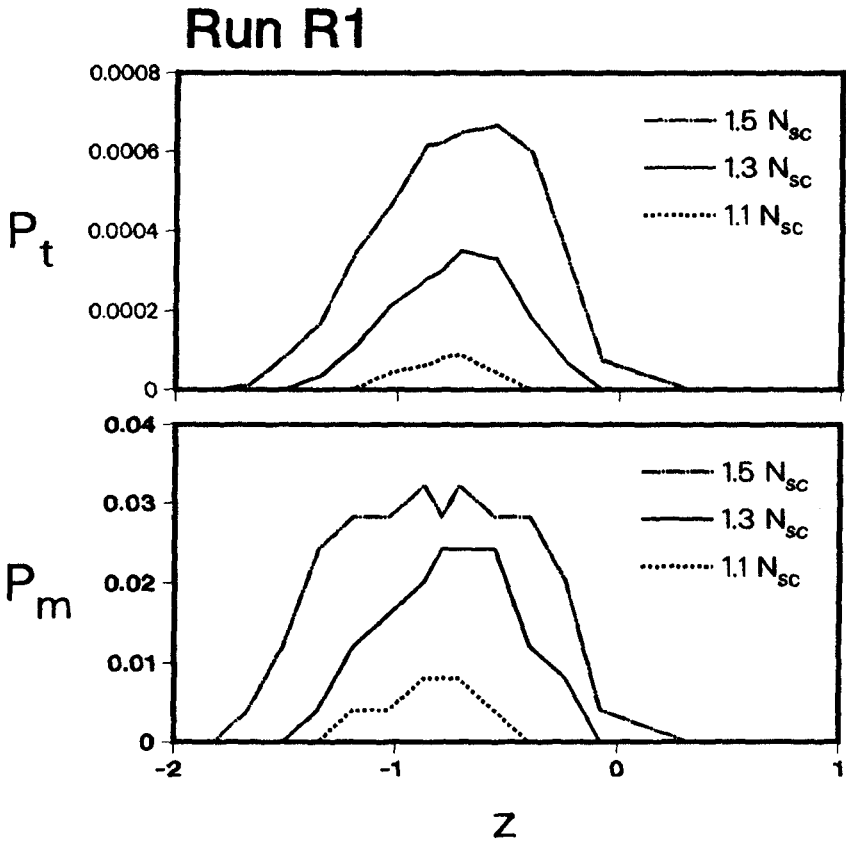


Figure 6: Computed Probabilities for Given N_s of Rock Movement for Run R1

movement of the armor units with $N_s = 1.72$, that is, $N_s/N_{sc} = 1.10$. However, the predicted probabilities for $N_s/N_{sc} = 1.1$ are very small as shown in Fig. 6.

The probability of armor dislodgement per unit normalized time, P_d , is expected to be less than P_m . As a first attempt, it is simply assumed that $P_d = C_d P_m$ where $C_d =$ empirical parameter. The rate of vertical erosion of the primary cover layer may be given by

$$\frac{\partial \eta'_e}{\partial t'} = \frac{C_3(d')^3}{1 - n_a} \frac{1 - n_a}{C_2(d')^2} \frac{P_d}{T'} = \frac{C_3 d' P_d}{C_2 T'} \tag{3}$$

where $\eta'_e =$ vertical erosion depth of the primary cover layer taken positive downward; $t' =$ time associated with the profile change; $d' =$ characteristic length of the armor unit; $C_3 =$ armor volume coefficient; $C_2 =$ armor area coefficient; $n_a =$ porosity of the primary cover layer; and $(P_d/T') =$ probability of dislodgement of a single unit per unit time. In Eq. 3, $C_3(d')^3/(1 - n_a)$ is the volume occupied by a single unit, while $(1 - n_a)/C_2(d')^2$ is the number of armor units per unit area along the slope. Eq. 3 predicts the erosion only since the dislodged armor units are assumed to be deposited in the region where P_d is essentially zero.

In the following, the profile change is assumed to be so small that P_d may be assumed to be independent of t' . Then, Eq. 3 yields $\eta'_e = (C_3 d' P_d t)/C_2$ where $\eta'_e = 0$ at $t' = 0$ and $t = t'/T'$ is the normalized time which is equal to the number of individual waves. Integration of η'_e along the slope in the region $\eta'_e > 0$ yields the eroded area A'_e . Van der Meer (1988) defined the damage level S by $S = A'_e/(W'/\rho_s)^{2/3}$. The present analysis can be shown to yield

$$S = \frac{C_d C_3^{2/3} (s - 1) N_s t}{C_2 \sin \theta'} \int P_m dz \tag{4}$$

where the stability number N_s is defined in Eq. 1 and the integration of P_m with respect to z can be performed for given $N_s > N_{sc}$ using the computed variation of P_m such as those shown in Fig. 6. For the runs listed in Table 1, use was made of $C_3 = 0.66$, $C_2 = 0.90$ and $s = 2.63$ by Kobayashi and Wurjanto (1990). In the following computation, the number of individual waves is taken to be $t = 1000$ and the value of N_s is varied such that $N_s/N_{sc} = 1.1, 1.2, \dots, 2.0$.

Fig. 7 shows the computed damage level S as a function of N_s for runs R1, R3 and R4. The empirical parameter C_d is taken as $C_d = 0.005, 0.01$ and 0.02 so that the computed values of S are of the order of the values of S based on the empirical formula of Van der Meer (1988) which is also plotted for each run in Fig. 7. The computed variations of S with respect to N_s for the other runs are also in qualitative agreement with the empirical formula. Eq. 4 will overestimate the value of S if S becomes so large that the profile change will result in the decrease in P_m and P_d . The major difference between Eq. 4 and the empirical formula is that the probability of armor movement P_m in Eq. 4 is computed for the specified incident wave train $\eta_i(t)$ for each run. It is hence possible to examine the sensitivity of P_m to various incident wave trains.

CONCLUSIONS

The computed results presented herein is not extensive and need to be verified. The numerical model is used to examine the detailed armor response to the specified incident wave trains since the detailed quantitative understanding

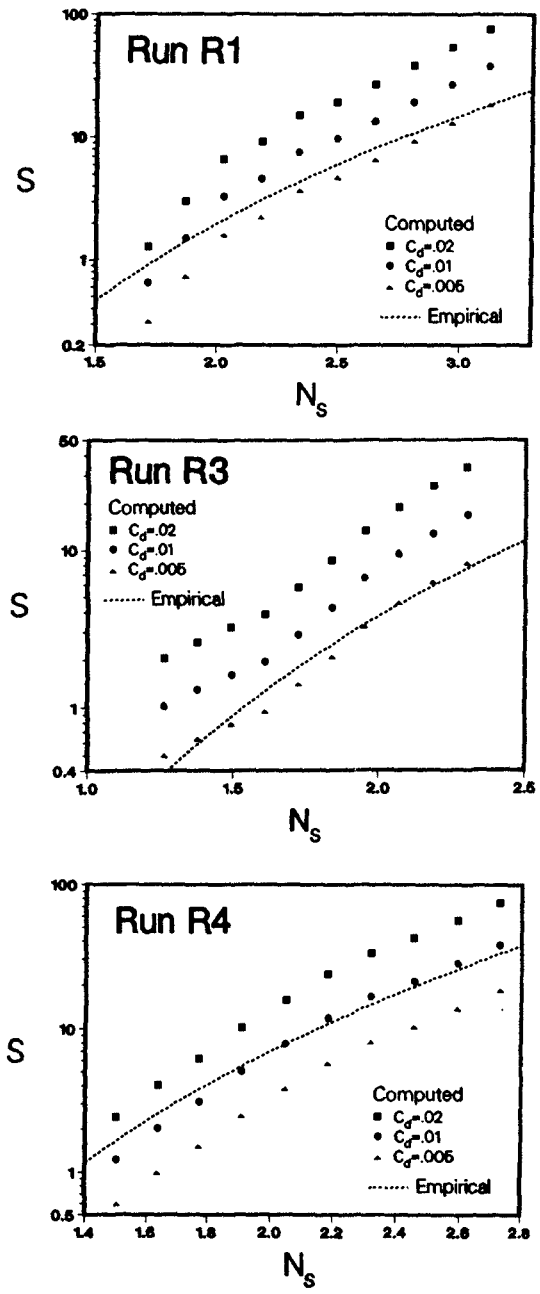


Figure 7: Computed Damage Level S as a Function of N_s for Runs R1, R3 and R4

is essential for improving the design of rock slopes for specified design waves as well as determining the design wave conditions more specifically than those based on the representative wave height and period. Generally, the scatter of data points about an empirical curve used for the design of a coastal structure against irregular waves is fairly large. Some of the scatter appears to be caused by the use of the representative wave height and period.

ACKNOWLEDGEMENT

This work is a result of research sponsored by Coastal Engineering Research Center, U.S. Army Engineer Waterways Experiment Station, under Contract No. DACW39-90-K-0006-P001 and the National Science Foundation, under grant CTS-8900640.

REFERENCES

- Gunbak, A. R. and Bruun, P. M. (1979), "Wave mechanics principles on the design of rubble-mound breakwaters." *Proc. P.O.A.C.*, Norwegian Inst. of Tech., Trondheim, Norway, 1301-1318.
- Kobayashi, N. and Wurjanto, A. (1989a), "Numerical model for design of impermeable coastal structures." *Res. Rept. No. CE-89-75*, Department of Civil Engineering, University of Delaware, Newark, DE 19716.
- Kobayashi, N. and Wurjanto, A. (1989b), "Armor stability on rough permeable slopes of marine structures." *Proc. 23rd I.A.H.R. Congress*, Ottawa, Canada, C, 407-414.
- Kobayashi, N. and Wurjanto, A. (1989c), "Numerical prediction of hydrodynamic forces and sliding motion of dolos units." *Proc. Stresses in Concrete Armor Units*, ASCE, 355-378.
- Kobayashi, N. and Wurjanto, A. (1990), "Numerical model for waves on rough permeable slopes." *J. Coast. Res.*, Special Issue No. 7 on Rational Design of Mound Structures, 149-166.
- Kobayashi, N., Wurjanto, A. and Cox, D.T. (1990), "Irregular waves on rough permeable slopes." *J. Coast. Res.*, Special Issue No. 7 on Rational Design of Mound Structures, 167-184.
- Kobayashi, N., Cox, D.T. and Wurjanto, A. (1990), "Irregular wave reflection and runup on rough impermeable slopes." *J. Wtrway. Port Coast. and Oc. Engrg.*, ASCE, 116(6) (in press).
- Van der Meer, J. W. (1988), "Rock slopes and gravel beaches under wave attack," Delft Univ. of Tech., Delft, The Netherlands, Doctoral Thesis.